Iran University of Science and Technology

Automotive Science and Engineering

Journal Homepage: ase.iust.ac.ir

ISSN: 2008-9899

Geometric Patterns Liquid Cooling System for Lithium-Ion Batteries in Electric Vehicles Considering Driving Cycle

Amirhossein jazari mamoei, Ayat Gharehghani *, Soheil Saeedipour

Department of Mechanical Engineering, Iran university of science and technology, Tehran, Iran.

* P.O.B. 123456789 Tehran, Iran, ayat_gharehghani@iust.ac.ir

ARTICLE INFO

Article history:

Received : 17 Mar 2024

Accepted: 13 May 2024

Published: 6 Jul 2024

Keywords:

Lithium-ion battery

Battery thermal management system

Microchannel

Heat transfer enhancement

Driving cycle

A B S T R A C T

A novel liquid cooling system for pouch-type lithium-ion batteries (LIBs) focuses on uniform temperature distribution and effective heat dissipation. The system utilizes a microchannel cold plate with an innovative coolant distribution design. The efficient microchannel design enhances thermal performance without incurring additional energy consumption. Additionally, using geometric patterns of cooling channels as an active cooling system improves thermal management performance. This study proposes a novel microchannel distribution path design, with each microchannel dimensioning 1 mm² and embedded in the battery's critical region to enhance the thermal contact among the LIB and the microchannels. This study aims to simulate and evaluate the performance of the cooling system under various Iranian environmental conditions (Tehran, Shiraz, Isfahan, and Bandar Abbas) and operational parameters (channel pattern, flow rate) to achieve optimal battery temperature and reduce energy consumption. Numerical investigations were conducted under 5C discharge conditions and a specific range of intake speeds (0.1m/s to 0.5m/s). The findings demonstrate that the designed liquid cooling successfully improves the thermal contact among the LIB and the liquid cooling in the battery cell's hot region around the channel outlet port. The proposed thermal management system reduces the maximum temperature (T_{max}) by 8K, and the maximum temperature difference (ΔT_{max}) is improved by 4.17K. Furthermore, the system's performance was evaluated under fluctuating heat generation rates, simulating real-world driving cycles. The study found that under varying driving conditions (based on the WLTP class 3 driving cycle), the T_{max} increased progressively, with periodic peaks and dips, reflecting the dynamic interaction between heat generation during high loads and the cooling system's efficiency. This demonstrates the system's capability to manage thermal fluctuations effectively during practical driving scenarios.

*Corresponding Author
Email Address: ayat_gharehghani@iust.ac.ir
https://doi.org/10.22068/ase.2024.678

[DOI: 10.22068/ase.2024.678]

Geometric Patterns Liquid Cooling System for Lithium-Ion Batteries in Electric Vehicles Considering Driving Cycle

1. Introduction

Lithium-ion batteries (LIBs) are highly significant with respect to energy density, voltage, cycle lifespan and discharge rate in comparison to alternative energy storage LIB. Alternative technologies include nickel-metal hydride (NiMH) and lead-acid batteries, which are cost-effective but lower in energy density. Their specific properties render them indispensable for Electric vehicles (EVs) and Energy storage system (ESS) [1,2]. Advancements in battery materials and architectures have led to a steady rise in the energy density of LIBs. By 2021, the average energy density had achieved 300 Wh/kg [3]. The rise in energy density has heightened the importance of thermal management for safety. Temperature plays an important role in determining the performance and longevity of LIBs. At lower temperatures, the reduction in chemical kinetic rate and at lower temperatures, the reduction in chemical interaction kinetics and the corresponding increase in internal resistance led to diminished battery capacity [4,5]. High temperatures encourage the failure of battery elements, resulting in diminished performance and a shortened lifespan. Moreover, high temperatures compromise thermal safety and can potentially trigger thermal runaway. [6,7]. The deployment of an effective battery thermal management system (BTMS) is necessary for ensuring the dependable operation of EVs. This system safeguards thermal stability, optimizes performance, and prolongs battery lifespan, thereby preventing the risk of thermal runaway [8,9]. Consequently, designing a system that regulates Keeping the cell temperature within the ideal range of 20°C to 50°C while improving temperature uniformity is crucial for efficient operation.

LIBs employ three primary thermal management system (TMS): hybrid, passive and active cooling. Active cooling consumes energy to regulate temperature through methods such as water- or air-based TMS [10,11]. In contrast, passive cooling maintains temperature without energy input, often based on materials with high thermal storage capacities, like PCM[12,13]. Numerous studies have focused on air-cooling methods and battery arrangement optimization. For example, the impact of air inlet position on the thermal behavior of cylindrical cells under forced air cooling has been investigated[14]. Xu et al.[15] investigated the impact of dual-side air inlet positioning on the thermal management of cylindrical cells under forced air cooling. Their results showed that the dual-side inlet design reduced the ΔT_{max} among the cells by approximately 20%, improving temperature uniformity and reducing the likelihood of hotspots. Additionally, this configuration decreased fan energy consumption by about 20%, enhancing cooling efficiency without increasing fan power demands. This approach not only improved thermal regulation within the battery pack but also offered an energy-saving advantage in cooling operations, making it a promising method for battery thermal management. Wang et al. [15] investigated air-cool BTMS efficiency in EVs by employing parallel plates. Their optimized design, consisting of two parallel plates with dimensions of 1.5mm in thickness and 30mm in height, yielded a T_{max} of 3.37K and a ΔT_{max} reduction of 5.5K above the ambient temperatue. Widyanthara et al. [16] introduced a variable fan system, examining the influence of air inlet temperature and the number of fans. Using the air-cooling methode, they modeled a 74 V, 2.31 kWh battery, revealing that the best performance, with minimal energy use, was achieved with three fans and a 25°C inlet temperature. While this setup successfully maintained all cells within the ideal temperature range, a ΔT_{max} of 15°C persisted. Liquid cooling systems, however, offer superior heat transfer efficiency compared to air cooling systems are preferred over air-cooling owing to the higher

[DOI: 10.22068/ase.2024.678]

thermal conductivity of liquids. These systems can cool module either directly using a high thermal conductivity fluid or indirectly through the use of a cooling plate [17,18]. Wang et al. [19] conducted a comparative analysis of the thermal efficiency between parallel and series flow configurations in BTMS. Their study revealed that parallel flow cooling resulted in a more uniform temperature distribution, maintaining a T_{max} below 36°C and limiting the ΔT_{max} to 4.17°C under 3C discharge rate. Li et al. [20] developed a lightweight U-shaped liquid cooling system for prismatic battery cells, which improved thermal safety and reduced weight. This system achieved a 21% reduction in T_{max} and a 45% decrease in the cooling plate's weight, making it particularly suitable for EV applications. Mangini and Thome [21] investigated the impact of Flow parameters on heat transfer during boiling in liquid cooling, finding that the presence of a thin liquid film significantly improved the thermal transfer coefficient. Li et al. [22] investigated the refrigerant flow configurations within a liquid cooling system, discovering that annular flow began at a lower quality with R1234ze than with R32 and R134a due to the lower vapor density of R1234ze. Jeyarajan et al. [23] investigated a spiral zigzag design for liquid cooling, optimizing six different configurations. Their five-channel design, with a width of 18mm, and a seven-channel design, with a width of 16mm, proved to be the most effective. The three-channel design had a peak outlet temperature of 330.84K. Wei et al. [24] focused on optimizing the heat transfer performance of liquid cooling with spiral channels for EV battery modules. Their findings demonstrated that, with pressure drops kept below 1000 Pa, the ΔT_{max} remained within the ranges of 0.29K, 1.11K, 2.17K, and 3.43K for discharge rates of 1C, 2C, 3C, and 4C, respectively. To further enhance heat transfer, Dong et al. [25] developed a wavy channel that lowered the T_{max} by 1.75°C in comparison to a conventional parallel channel pattern. Lee and Garimella [26] conducted a study on saturated flow boiling heat transfer in microchannel heat sinks (MCHS) and found that the pressure drop increased significantly with higher flow rates. additionally, the local heat transfer coefficient rose almost linearly at low to moderate levels of heat flux. Li et al. [27] introduced data on the heat transfer coefficient and pressure drop of R32 in a cold plate, showing that R32 provided a higher heat transfer coefficient and lower pressure compared to R134a. Lin et al. [28] introduced a silicone gel and cross-structured cold plate system, achieving a temperature of below 45°C and a ΔT_{max} within 2°C at a 3C discharge rate. Worwood et al. [29] proposed a graphite for Cooling of high-capacity LIBs, achieving an in-plane thermal conductivity five times greater than that of aluminum, without adding extra weight. Their results indicated an 8°C reduction in peak temperatures and a 5°C decrease in surface temperature gradients compared to aluminum fins during aggressive EV cycles.

In contrast to active thermal management methods, passive cooling systems do not consume energy and primarily rely on heat pipes and PCMs. These materials absorb significant heat during phase transitions with minimal volume change. Additives with high thermal conductivity are often merge into PCM composites to improve thermal conductivity [30]. Huang et al. [31] developed a flexible composite phase change material (CPCM) that reduced contact resistance in BTMS, decreasing the temperature by 10°C. Choudhary et al. [32] investigated numerical analyses of battery packs with finned structures and PCMs, finding that finned structures improved heat transfer efficiency and reduced T_{max} by 8.17%. Rabiei et al. [33] explored various liquid cooling configurations, including Corrugated plate and embedded foam metal cold plate. Their results showed that wavy wall cold plate provided

[DOI: 10.22068/ase.2024.678]

superior heat dissipation at higher inlet velocities, while foam metal cold plate offered better cooling and lower energy consumption at lower velocities. Ki et al. [34] investigated a cooling path for a battery pack, achieving ideal temperature control and a temperature difference of less than 2°C at 4.2 times lower flow rates. In research operated by Wang et al. [35] tested several fin designs, for use in PCM chambers. Their results demonstrated that the X-shaped fin, with its branching structure, delivered the best thermal performance. A summary of the articles and their important findings are shown in Table 1.

This work proposes a novel liquid cooling system utilizing a cold plate for the TMS of pouch-type LIBs, featuring an optimized coolant design. The primary goals are to ensure a homogeneous temperature distribution throughout the battery surface and to facilitate efficient thermal dissipation, both of which are essential for optimal thermal management in LIBs. The study also aims to minimize energy consumption while achieving an optimal T_{max} through an active cooling system based on cold plate technology. This system includes an inlet/outlet and a thermally conductive plate. The analysis evaluates the influence of operational parameters, including varying environmental temperatures across different cities in Iran (Tehran, Shiraz, Isfahan, and Bandar Abbas), as well as different geometric cooling channel patterns and flow rates, on system performance. Additionally, temperature variations across the battery module and T_{max} are analyzed to guarantee optimal thermal efficiency and mitigate potential safety risks.

2. Materials and Method

The LIB cell used in this study is commonly found in commercial EVs, such as the Volkswagen and BMW i3. It features a carbon electrolyte, copper cathode, and aluminum anode, with a dimension of 45mm in width, capacity of 7Ah, 9mm in thickness and 145mm in height. The specifications of the battery and cooling plate are outlined in Tables 1 and 2. The analysis was performed on a module comprising three battery cells and two cooling plates (Figure 1). The cooling plate features an inlet cross-sectional area of 1mm². Additionally, a Poorest-sample plan with a 5C discharge rate was modeled to compare the TMS, with a user define function (UDF) code used to calculate transient heat generation.

Table 1: A summary of the articles and their important findings

author	Cooling Method	Key Features	Performance Metrics	Observations
Wang et al. [17,18]	Air Cooling	Parallel plates (1.5mm thick, 30mm high)	T_{max}:3.37K, ΔT_{max}:5.5K above ambient	Optimized design reduces temperature rise above ambient, improving cooling efficiency.
Wid et al. [16]	Air Cooling	Variable fan system with 74V, 2.31kWh battery model	Best at 25°C inlet temp with three fans, ΔT_{max}: 15°C	Maintains cells in ideal temp range, though temperature difference remains significant.
Wang et al. [19]	Liquid Cooling	Parallel vs. series flow configurations	Parallel: T_{max}< 36°C, ΔT_{max}: 4.17°C at 3C	Parallel flow yields more uniform temperature than series flow at high discharge rates.
Li et al. [20]	Liquid Cooling	Lightweight U-shaped system for prismatic cells	21% T_{max}reduction, 45% weight decrease	Enhances thermal safety and reduces system weight, ideal for EV applications.
Mangini & Thome [21]	Liquid Cooling	Boiling heat transfer with thin liquid film	Improved thermal transfer coefficient	Thin film enhances heat transfer, beneficial for high-efficiency cooling.

[DOI: 10.22068/ase.2024.678]

Table 1: A summary of the articles and their important findings

author	Cooling Method	Key Features	Performance Metrics	Observations
Li et al. [22]	Liquid Cooling	R1234ze refrigerant with annular flow	Initiates at lower quality compared to R32, R134a	R1234ze has lower vapor density, enhancing cooling efficiency at lower qualities.
Jeyarajan et al. [23]	Liquid Cooling	Spiral zigzag design, optimized for multiple configurations	Best at five-channel (18mm) and seven-channel (16mm) widths; 3-channel: T_outlet = 330.84K	Optimized design improves cooling efficiency in spiral zigzag configurations.
Wei et al. [24]	Liquid Cooling	Spiral channels with controlled pressure drops	ΔT_{max}: 0.29K (1C), 1.11K (2C), 2.17K (3C), 3.43K (4C)	Maintains low temp differentials across discharge rates under pressure drop constraints.

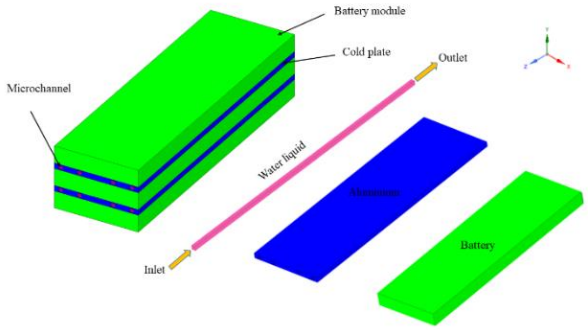

Figure 1: the design of the LIBs module, the cold plates, and the positioning of the liquid cooling

Table 2: Battery Cell Specifications [36]

Parameter	Value
Capacity (mAh)	7000
Nominal Voltage (V)	3.8
Density (kg/m³)	2263
Positive Electrode Material	Aluminum
Negative Electrode Material	Copper
Specific Heat Capacity (J/kg·K)	1523
Thermal Conductivity (W/m·K)	$k_r = 21.3, k_\theta = 21.3$ $k_z = 21.3$
Nominal Voltage (V)	3.8
Operating Temperature (°C)	10 - 45

Table 3: properties of cold plate(aluminium)

Parameter	Value
Size (mm)	451 × 453
Thermal Conductivity (W/m·K)	202.4
Specific Heat Capacity (J/kg·K)	871
Density (kg/m³)	2719

[DOI: 10.22068/ase.2024.678]

3. Equations

The computational domain is segmented into three distinct subdomains: the battery cell, the cold plate (constructed of aluminum) and the fluid section (comprising water). Each of these subdomains is governed by a unique set of equations, which are formulated to address their specific thermal and fluid dynamics properties.

3.1. Battery

For the battery cell, heat generation is influenced by a range of factors, including cell size, state of charge (SOC), discharge rate, temperature, and the rate of electrochemical reactions. In this study, the heat generation model relies on the relationship established by Bernardi et al. [37], which links thermal generation to key electrical parameters. By integrating this model with the thermodynamic energy equation, new insights and results were derived for a full cell system, improving the understanding of thermal behavior under varying operational conditions.

$$\dot{Q} = I(U - V) - I(T\frac{\partial U}{\partial T}) \quad (1)$$

The parameters U, $\dot{Q}$,T, I and V in the equation present the open-circuit voltage of the cell, heat generation, cell temperature, current and voltage, respectively. The above equation can be rewritten according to previous studies [38] as follows:

$$\dot{q} = R_i i^2 - iT\frac{\Delta S}{F} \quad (2)$$

In the given equation i, ΔS, $\dot{q}$, R_i and F represent the cell discharge current, entropy change, internal heat production rate, internal equivalent resistance, and Faraday's constant, respectively. The inner equivalent resistance is influenced by temperature and the SOC.

The SOC is defined as follows:

$$SOC = 1 - \frac{I \cdot t}{C_0} \quad (3)$$

Battery energy equation: I indicate the discharge current; t denotes the discharge duration and C_0 refers to the nominal battery capacity:

$$\frac{\partial}{\partial t}(\rho_b C_{p,b} T_b) = \nabla \cdot (k_b \nabla T_b) + \dot{q} \quad (4)$$

Here, ρ_b, k_b, $C_{p,b}$ are the density, thermal conductivity and specific heat capacity respectively.

3.2. Cooling Fluid

The fluid part of the BTMS is governed by the mass conservation, flow, and energy equations and is rewritten as follows [39]:

$$\frac{\partial \rho_f}{\partial t} + \nabla \cdot (\rho_f \vec{v}) = 0 \quad (5)$$

$$\frac{\partial}{\partial t}(\rho_f \vec{v}) + \nabla \cdot (\rho_f \vec{v}\vec{v}) = - \nabla p + \nabla \cdot (\bar{\bar{\tau}}) \quad (6)$$

3.3. Cooling Plate

The energy balance equation governing the cooling plate is mathematically represented as follows [40]:

$$\frac{\partial}{\partial t}(\rho_s C_{p,s} T_s) = \nabla \cdot (k_s \nabla T_s) \quad (7)$$

Here $C_{p,s}$, k_s and ρ_s represent the heat capacity, thermal conductivity and density respectively.

4. Initial and boundary conditions

CFD simulations were conducted to investigate battery cooling using microchannels. Initially, the entire domain was subjected to the ambient temperature condition. Then, four ambient conditions corresponding to the cities of Tehran, Shiraz, Isfahan, and Bandar Abbas, with temperatures of 295K, 298K, 301K, and 304K respectively, were simulated[41]. By applying the boundary conditions, the inlet speed (ranging from 0.1 to 0.5m/s) and the outlet pressure (ambient pressure) were kept constant. The inlet fluid temperature in each simulation was matched to the ambient temperature.

5. Numerical Methods and Grid Independence

ANSYS Fluent was employed to conduct the CFD simulation, utilizing a hexahedral mesh to

[DOI: 10.22068/ase.2024.678]

enhance analysis precision. The governing equations were resolved via a pressure-based solver, with pressure-velocity coupling managed through the SIMPLE algorithm. A UDF was implemented to calculate the internal heat production of the cell, based on well-established mathematical models. To confirm grid independence, four mesh sizes (32,154; 57,372; 88,596; and 115,782 elements) were tested. During the discharge process at a 5C rate, with an ambient temperature of 298K and a fluid velocity of 0.3m/s, the T_{max} and the temperature difference ΔT_{max} at 720 seconds(The simulation was also performed in an transient) exhibited variations of less than 5% and 5.7%, respectively, between the two finest meshes. These findings are depicted in Figure 2, which highlights the variation in T_{max} and ΔT_{max} across the different mesh sizes.

Table 4: schemes and approximations done within simulation.

Simulation Parameter	Method/Approach
Mesh Type	Hexahedral Mesh
Mesh Sizes Tested	32,154; 57,372; 88,596; 115,782 elements
Solver Type	Pressure-Based Solver
Pressure-Velocity Coupling	SIMPLE Algorithm
Pressure	2nd Order
Momentum	2nd Order Upwind
Energy	2nd Order Upwind
Time Step	Based on Courant-Friedrichs-Lewy (CFL) condition
Grid Independence Study	Conducted with four mesh sizes; T_{max} and ΔT_{max} varied by less than 5% for the two finest meshes
Boundary Conditions	Inlet velocity: 0.3 m/s; Ambient Temperature: 298K
UDF	Used to calculate internal heat generation based on mathematical model
Simulation Duration	720 seconds at 5C discharge rate

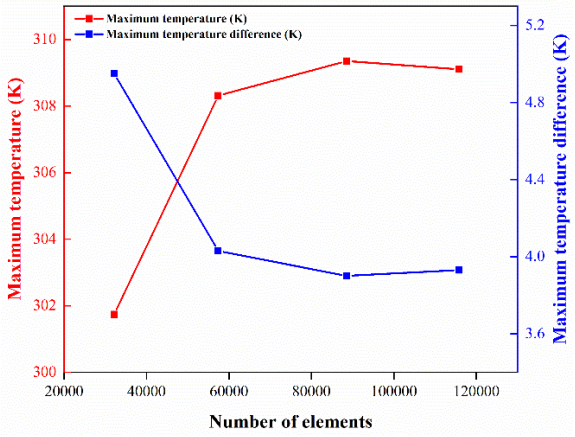

Figure 2: Grid independence test during the 5C discharge rate

6. Validation of the Numerical Model

In this research, validation was carried out separately for both the LIB cell domain and the cooling section due to the distinct parts involved. The validation procedure involved comparing the average temperature of a 100Ah LIB subjected to normal air cooling at two distinct discharge rates, beginning from a primary temperature of 293K, with a convective thermal transfer coefficient of 5 W/m²K. data from Lin et al. [42] were incorporated into this comparison, as depicted in Figure 3. Additionally, a comparison was conducted between the results for a straight-walled liquid cooling and the discovering from Fan et al. [43]examining different flow rates during a 600-second discharge process at a surrounding temperature of 300K. These evaluation results are summarized in Table 5, with the maximum deviation observed for standard temperature deviation being 2.92%, indicating strong agreement between the simulation and experimental data. The standard temperature digression is computed as follows:

$$STD = \sqrt{\frac{(T_{max} - T_{avg})^2 + (T_{min} - T_{avg})^2}{2}} \quad (8)$$

[DOI: 10.22068/ase.2024.678]

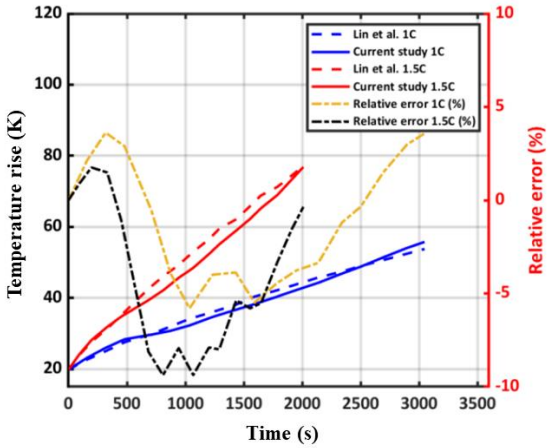

Figure 3: Comparison of experimental and numerical results for the average battery temperature rise[44].

Table 3: Evaluation of standard heat deviation inside LIB

Flow Rate (m^3/h)	Present Study	Fan et al. [43]	Difference (%)
1.2	1.149	1.143	2.55
1.4	1.272	1.263	3.92
1.6	1.349	1.356	2.39
1.8	1.485	1.485	1.92

7. Results and discussion

This part offers a numeral analysis of the suggested cold plate for a pouch-type LIBs under high discharge rates (5C) using water cooling with varying inlet velocities from 0.1m/s to 0.5m/s and four environmental conditions in Iran with average temperatures of 295K, 298K, 301K, and 304K, under different microchannel geometric patterns.

7.1 Performance of the enhanced BTMS

In this part, the efficiency of the suggest BTMS is evaluated by change the cooling pump speed under a 5C rate and an inlet fluid temperature of 298K. Based on this hypothesis, the inlet velocities, expressed in terms of Reynolds numbers, are presented in Table 4. The flow regime is determined based on the Reynolds number. As shown in Table 4, the Reynolds numbers are less than 2300, indicating a laminar flow regime. Figure 4 shows the behaviour of the T_{max} over time and compares the temperature monotony of the module at various inlet speeds. As the flow rate increases, T_{max} during the discharge process gradually rises, becoming more noticeable after the first 60 seconds (Figure 4a). Additionally, the temperature difference increases with higher flow velocities, leading to reduced uniformity in the battery module (Figure 4b). During the early stages of discharge, after 80 seconds, the cooling fluid significantly reduces the T_{max} due to the thermal conductivity of the cooling plate and the convective heat transfer coefficient of water. For inlet velocities of 0.1, 0.2, 0.3, 0.4, and 0.5m/s, the maximum temperatures were 309.8K, 308.7K, 308.3K, 308.1K, and 307.8K, respectively. Therefore, a mean Reynolds number of 813.24, corresponding to an inlet velocity of 0.3m/s, was selected for further analysis.

Table4: Comparison of Inlet Flow Speed by Reynolds Number

Speed (m/s)	Reynolds Number
0.1	2771.08
0.2	5441.6
0.3	8123.4
0.4	10842.2
0.5	13557.4

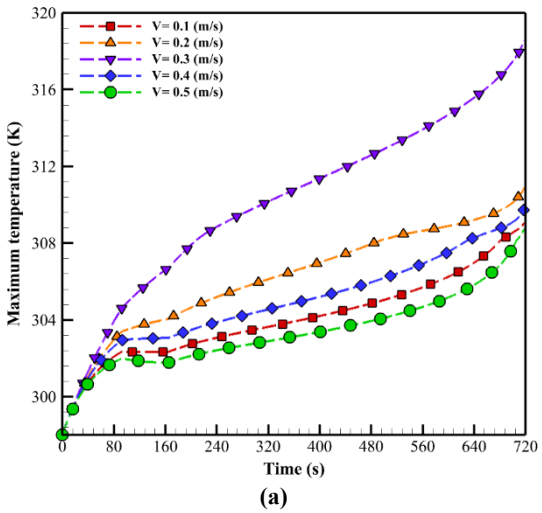

(a)

[DOI: 10.22068/ase.2024.678]

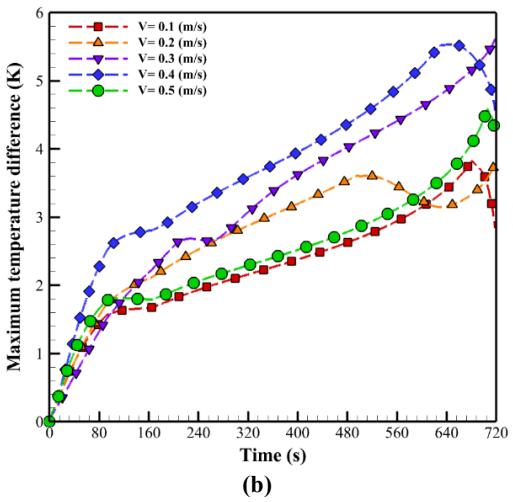

Figure 4: distribution diagram of (a) T_{max} and (b) ΔT_{max} with different speed values

7.2 Analysis of environmental conditions

EVs must perform reliably across a range of environmental conditions and evaluates the thermal efficiency of the proposed cooling systems, with a focus on their performance at varying ambient temperatures: 295K (Tehran), 298K (Shiraz), 301K (Isfahan), and 304K (Bandar Abbas), under a 5C discharge rate and a specific inlet speed of 0.3m/s. Figure 5 presents a bar chart showing the T_{max} and ΔT_{max} of the battery under these four environmental conditions for the proposed cooling system. Water, without pre-cooling, enters the microchannels, achieving thermal equilibrium at the ambient temperature. As the ambient temperature increases, the maximum temperature rises across all environmental conditions. Notably, as the environment becomes warmer, a decreasing trend in temperature difference is observed, attributed to the higher ambient temperature. At an inlet velocity of 0.3m/s and under variable temperatures of 295K, 298K, 301K, and 304K with a 5C discharge rate, the T_{max} recorded were 305.6K, 308.6K, 309.2K, and 310.9K, respectively. Additionally, the ΔT_{max}, 4.32K, 4.03K, 2.84K, and 2.26K remained below 5K. Figure 6 illustrates temperature distribution in a battery module under ambient temperatures of 295K, 298K, 301K, and 304K. As ambient temperature rises, the module's T_{max} also increases, reaching 310.9K at 304K. ΔT_{max} decreases with higher ambient temperatures, suggesting more uniform cooling. The cooling system keeps ΔT_{max} below 5K, indicating effective thermal management across various conditions.

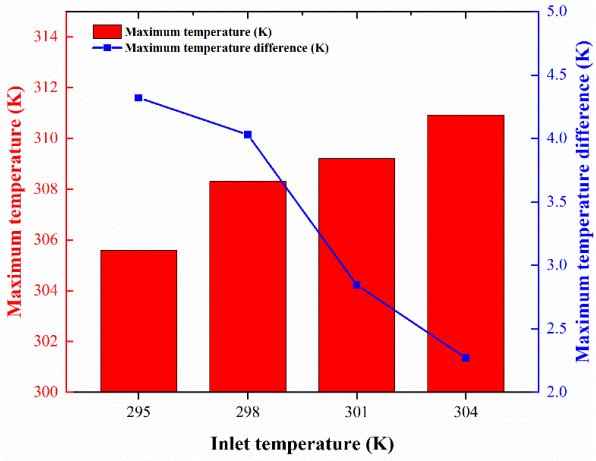

Figure 5: Bar chart of T_{max} and ΔT_{max} under various ambient temperatures

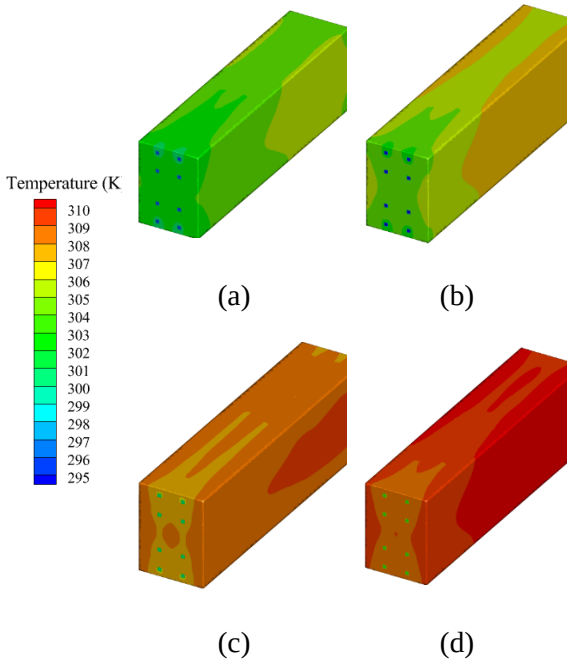

Figure 6: Temperature distribution contour of the module under various environmental conditions, (a)295K, (b)298K, (c)301K, (d)304K

[DOI: 10.22068/ase.2024.678]

7.3 Analysis and evaluation of cooling channel geometric patterns

In this part, the evaluation of the placement of microchannels and the effect of the number of microchannels have been examined.

7.3.1 Effect of the number of microchannels

In this part, the thermal efficiency of the planed cooling system is evaluated based on the number of microchannels and its impact on the battery's thermal performance, as shown in Figure 7. The simulation was conducted at an ambient temperature of 298K and an inlet velocity of 0.3m/s. Figure 8 presents a bar chart of the T_{max} and ΔT_{max} of the LIB in relation to the number of microchannels for the proposed cooling system. As the number of microchannels increases, the contact area between the coolant and the battery rises. This leads to an enhanced heat transfer rate, consequence in a reduction in battery temperature. At an inlet velocity of 0.3m/s, the T_{max} for configurations with 2, 4, 6, and 8 microchannels were 318.59K, 310.89K, 309.05K, and 308.31K, respectively. Additionally, the ΔT_{max} recorded were 5.61K, 3.78K, 2.84K, and 2.43K.

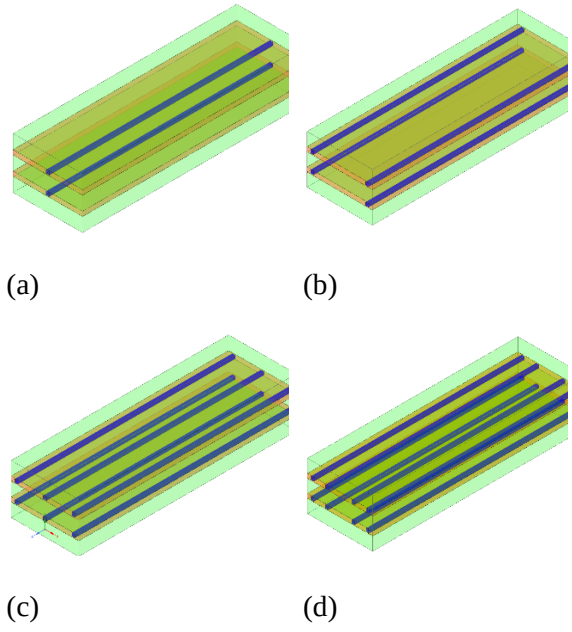

Figure 7: Schematic of the evaluated microchannels: (a) 2 microchannels, (b)4 microchannels, (c) 6 microchannels, (d) 8 microchannels

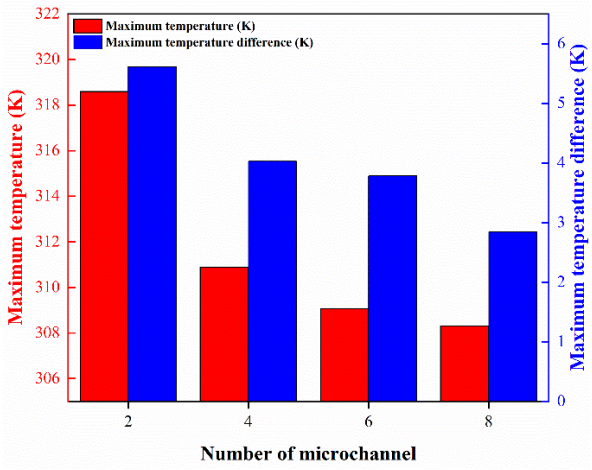

Figure 8: Bar chart of T_{max} and ΔT_{max} for the battery module with varying numbers of microchannels

7.3.2 Microchannel arrangement

The thermal efficiency of the optimized cooling systems is evaluated based on the arrangement of the microchannels in two configurations: horizontal and vertical, under ambient conditions of 298K and an inlet velocity of 0.3m/s. Figure 9 presents behavior showing the T_{max} and ΔT_{max} of the LIB relative to the microchannel arrangement (horizontal and vertical) for the proposed cooling system. The vertical microchannel configuration exhibits better thermal performance compared to the horizontal arrangement due to improved contact area between the microchannel and the battery, and the more efficient convective heat transfer coefficient of water. T_{max} for the horizontal and vertical arrangements were 316.30K and 308.31K, respectively, and the T_{max} were 8.20K and 4.03K, respectively. In terms of T_{max} and ΔT_{max}, the vertical arrangement showed approximately 2.52% and 50% better performance compared to the horizontal arrangement. Figure 10 shows the temperature contour in horizontal and vertical arrangements, as it is clear that the vertical arrangement has a

[DOI: 10.22068/ase.2024.678]

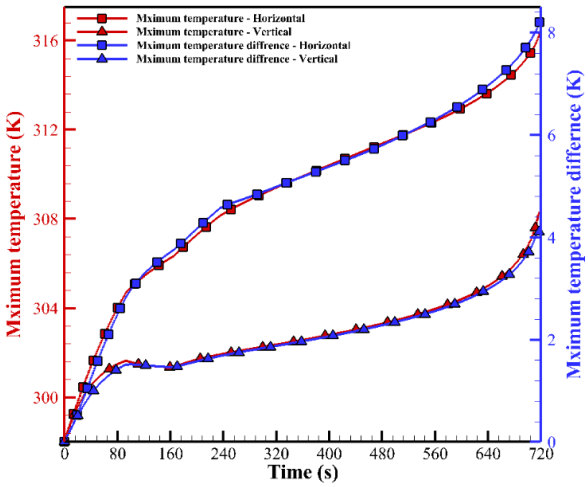

Fig 9: distribution behavior of T_{max} and ΔT_{max} in the battery pack with variable microchannel geometric arrangements

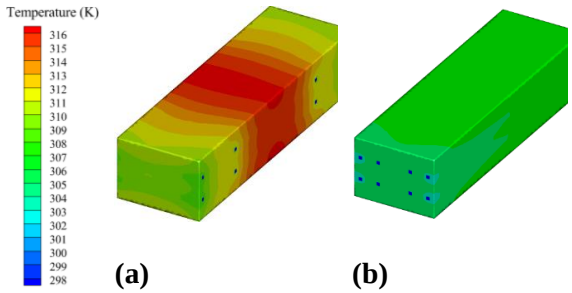

Figure 10: Temperature distribution for the battery module with different geometric patterns

lower temperature than the horizontal arrangement.

7.4 Driving cycle

Recent researches have primarily emphasized on evaluating the efficiency of BTMS under constant heat production rates or constant discharge rates. However, actual thermal production in LIBs is closely tied to driving behavior, leading to notable oscillations. This section addresses oscillating heat production as a representative condition of real-world battery operation and examines the efficiency of BTMS under these dynamic conditions. Based on data for heat production in LIBs during the driving cycle (WLTP class 3) [45], the volumetric heat production rate was determined. Figure 11(a) illustrates the heat generation rate at different driving intervals, with the rate peaking at 190,000 W/m³ and exhibiting oscillatory behavior throughout the. The ΔT_{max} and the ΔT_{max} at three different inlet temperatures (295K, 298K, and 301K) are presented in Figures 11(b), 11(c), and 11(d), respectively. The T_{max} increases from 295K to 304K, from 298K to 307K, and from 301K to 310K. The periodic peaks and dips over time indicate a balanced interaction between heat generation during high loads and cooling mechanisms. The ΔT_{max} follows a similar pattern, peaking at approximately 1K, which indicates uneven heat distribution in the LIBs. Figure 12 presented the temperature contours at the three initial temperatures (295K, 298K, and 301K), with final temperatures of 307K, 306K, and 305.5K, respectively. The driving range and battery charging time are key determinants of the overall user experience in EVs. This research presents an innovative battery module architecture, incorporating a dense cell configuration and an optimized thermal management system to enhance the energy capacity of the LIB pack, thereby extending the EV's driving range. Furthermore, the implementation of an elevated charge/discharge rate in this design reduces the time required for battery charging.

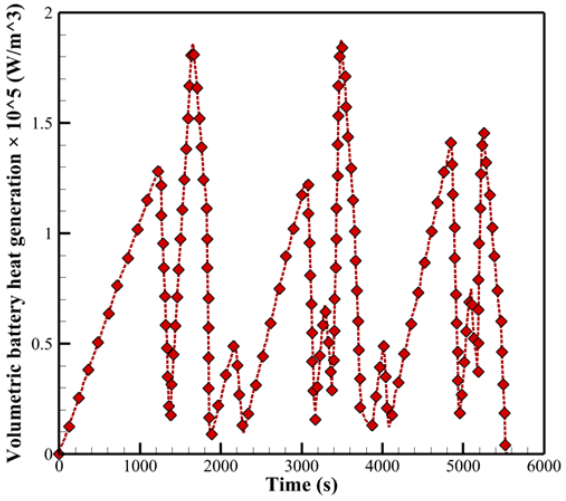

(a)

[DOI: 10.22068/ase.2024.678]

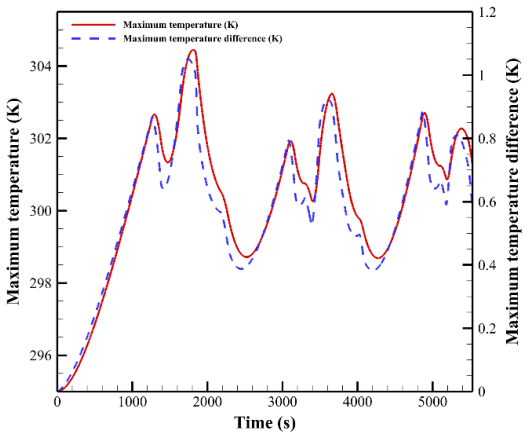

(b)

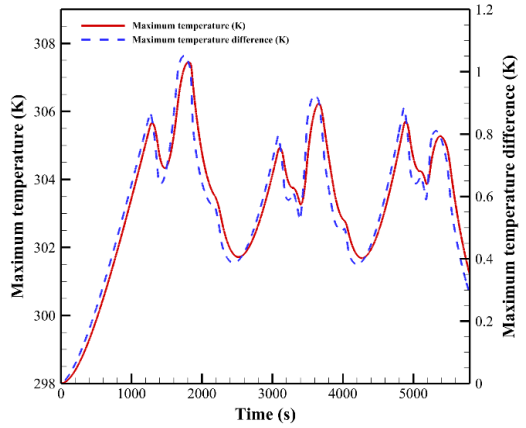

(c)

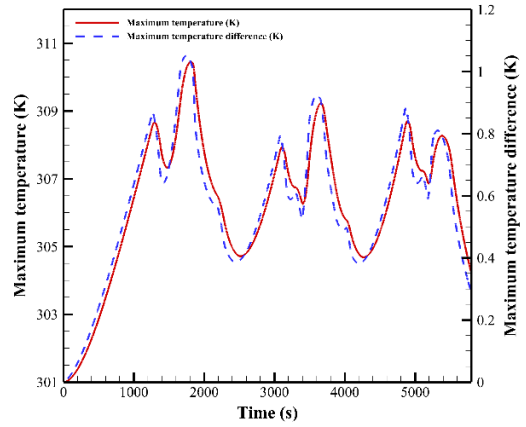

(d)

Figure 11: (a) Battery heat generation rate during the driving cycle[45], distribution behavior of T_{max} and ΔT_{max} at 0.3 m/s at (b) 295K, (c) 298K, (d) 301K

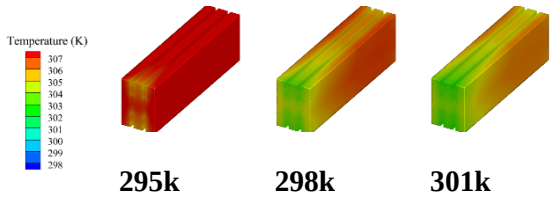

Figure 12. Module temperature distribution contour under three different input temperatures in the driving cycle

7.4 Analysis of pressure drop and energy consumption

In this section, the pressure drop and energy consumption are analyzed based on inlet velocities in the microchannels. As shown in Figure 13, the pressure drops increases significantly with higher inlet velocities. This is due to the increased flow resistance as the fluid moves faster through the channels. Specifically, the pressure drop increases sixfold when the speeds is raised from 0.1m/s to 0.5m/s. Similarly, energy consumption rises with increasing inlet velocity. This is attributed to the higher energy losses from friction in the flow. As the inlet speed increases from 0.1m/s to 0.5m/s, energy consumption also increases by a factor of six.

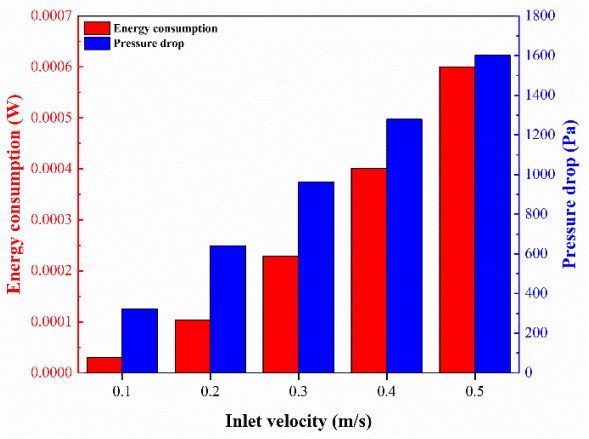

Fig 13: Pressure drop and energy consumption based on different inlet velocities in the microchannels

[DOI: 10.22068/ase.2024.678]

8. Conclusion

In this discussion, a cooling system was suggested to dissipate the heat generated from a 7Ah LIB module. The performance of liquid cooling at a 5C discharge rate demonstrated that the proposed system can successfully hold and meliorate temperature monotony within the optimal limit. Key factors such as the performance of the thermal management system, microchannel arrangement, the number of microchannels, and environmental conditions were examined to assess their impact on battery pack performance. The findings are summarized as follows:

1)Numerical simulations were performed under four environmental conditions in Iran: 295K (Tehran), 298K (Shiraz), 301K (Isfahan), and 304K (Bandar Abbas), with an intake speed of 0.3m/s and a 5C discharge rate. As ambient temperature increased ,the ΔT_{max} increased, but theΔT_{max} decreased. The T_{max} for the respective ambient conditions were 305.6K, 308.6K, 309.2K, and 310.9K

2)The analysis of microchannel orientation (horizontal vs. vertical) showed that the vertical arrangement provided 50% better cooling performance due to increased contact area and a higher convective heat transfer coefficient. The T_{max} and ΔT_{max} for the vertical configuration were 308.31K and 4.03K, while for the horizontal configuration, they were 316.30K and 8.20K, respectively.

3)As the inlet velocity increased, the $\mathbf{T_{max}}$during discharge decreased, while the $\mathbf{\Delta T_{max}}$ increased. In the early stages of discharge (after 80 seconds), the cooling fluid had a significant impact on reducing $\mathbf{T_{max}}$.

4)Increasing the number of microchannels resulted in greater contact area with the coolant and an enhanced heat transfer rate. At an inlet velocity of 0.3m/s, the $\mathbf{T_{max}}$ for 2, 4, 6, and 8 microchannels were 318.59K, 310.89K, 309.05K, and 308.31K, respectively.

5)The hybrid BTMS can improve the thermal performance of the BTMS using passive cooling strategies that do not consume energy. However, inserting PCMs to the BTMS must be limited based on the overall weight of TMS. The adoption and mass of PCM in this study can be optimized in future research to achieve the best thermal efficiency with an optimal PCM weight.

6)The pressure drop and energy consumption were analysed based on different inlet velocities in the microchannels. As inlet velocity increased, the pressure drop rose significantly due to the greater flow resistance at higher velocities. The pressure drops increased sixfold when the intake speed increased from 0.1m/s to 0.5m/s. Similarly, energy consumption increased with inlet velocity due to higher energy losses from friction and turbulence. As the inlet velocity increased from 0.1m/s to 0.5m/s, energy consumption also increased sixfold.

7) The efficiency of the BTMS was figure out under situation that considered oscillating heat generation, representing real-world battery operating scenarios. The ΔT_{max} increased from 295K to 304K, 298K to 307K, and 301K to 310K. The T_{max} followed a similar pattern, peaking at approximately 1K, indicating the presence of uneven heat distribution within the battery cells.

Numen culture

c	Charge rate (C)
Re	Reynolds number
k	Thermal conductivity coefficient (W/m.k)
ΔT_{max}	Maximum temperature difference (K)
t	Time (s)
V	Velocity (m/s)
T_{max}	Maximum temperature (K)
Q_{gen}	Heat production (W)
R	Internal resistance (Ω)
U	Battery voltage (v)
I	Current (A)

[DOI: 10.22068/ase.2024.678]

m	Mass (kg)
v	Voltage (v)

Greek symbols

ρ	Density (kg/m3)
μ	Dynamic viscosity (kg/ms)

Abbreviation

BTMS	Battery thermal management system
SOC	Charging mode
PPI	Pores per inch
LIB	Lithium-ion battery
TMS	Thermal management system
CFD	Computational fluid dynamics
UDF	User-defined functionality
STD	Standard deviation of temperature
CPCM	Composite phase change material

References

[1] Y. Zhao, B. Zou, T. Zhang, Z. Jiang, J. Ding, Y. Ding, A comprehensive review of composite phase change material based thermal management system for lithium-ion batteries, Renewable and Sustainable Energy Reviews 167 (2022) 112667. https://doi.org/10.1016/j.rser.2022.112667.

[2] M. Rabiei, A. Gharehghani, S. Saeedipour, Novel hybrid BTMS by considering safety and driving cycle under extreme fast charge/discharge rates, J Energy Storage 99 (2024) 113486. https://doi.org/10.1016/j.est.2024.113486.

[3] W. Li, Y. Zhou, H. Zhang, X. Tang, A Review on Battery Thermal Management for New Energy Vehicles, Energies (Basel) 16 (2023) 4845. https://doi.org/10.3390/en16134845.

[4] A. Belgibayeva, A. Rakhmetova, M. Rakhatkyzy, M. Kairova, I. Mukushev, N. Issatayev, G. Kalimuldina, A. Nurpeissova, Y.K. Sun, Z. Bakenov, Lithium-ion batteries for low-temperature applications: Limiting factors and solutions, J Power Sources 557 (2023). https://doi.org/10.1016/j.jpowsour.2022.232550.

[5] X. Su, Y. Xu, Y. Wu, H. Li, J. Yang, Y. Liao, R. Qu, Z. Zhang, Liquid electrolytes for low-temperature lithium batteries: main limitations, current advances, and future perspectives, Energy Storage Mater 56 (2023) 642–663. https://doi.org/10.1016/j.ensm.2023.01.044.

[6] C. Liu, X. Wen, J. Zhong, W. Liu, J. Chen, J. Zhang, Z. Wang, Q. Liao, Characterization of aging mechanisms and state of health for second-life 21700 ternary lithium-ion battery, J Energy Storage 55 (2022). https://doi.org/10.1016/j.est.2022.105511.

[DOI: 10.22068/ase.2024.678]

[7] S. Xie, X. Yang, Q. Sun, Z. Wang, Y. He, Research progress and prospects on thermal safety of lithium-ion batteries in aviation low-temperature and low-pressure environments, J Energy Storage 83 (2024) 110734. https://doi.org/10.1016/j.est.2024.110734.

[8] R. Peng, D. Kong, P. Ping, G. Wang, X. Gao, H. Lv, H. Zhao, X. He, Y. Zhang, X. Dai, Thermal runaway modeling of lithium-ion batteries at different scales: Recent advances and perspectives, Energy Storage Mater 69 (2024). https://doi.org/10.1016/j.ensm.2024.103417.

[9] S. Saeedipour, A. Gharehghani, J. Ahbabi Saray, A.M. Andwari, M. Mikulski, Proposing a Hybrid Thermal Management System Based on Phase Change Material/Metal Foam for Lithium-Ion Batteries, World Electric Vehicle Journal 14 (2023) 240. https://doi.org/10.3390/wevj14090240.

[10] Y. Xie, L. Li, Q. Xu, X. Li, H. Huang, Y. Huang, S. Bei, L. Zhang, K. Zheng, Effects of module size on the heat dissipation performance of the thermal management system for the battery module with cylindrical cells, Appl Therm Eng 238 (2024). https://doi.org/10.1016/j.applthermaleng.2023.121958.

[11] A. Gharehghani, M. Rabiei, S. Mehranfar, S. Saeedipour, A. Mahmoudzadeh Andwari, A. García, C.M. Reche, Progress in battery thermal management systems technologies for electric vehicles, Renewable and Sustainable Energy Reviews 202 (2024) 114654. https://doi.org/10.1016/j.rser.2024.114654.

[12] Z. Huiming, T. Zuohang, Y. Tianyang, T. Changqing, Review of Research on Thermal Management Technology for Electric Vehicles, Journal of Refrigeration 43 (2022) 15–27. https://doi.org/10.3969/j.issn.0253-4339.2022.03.015.

[13] S. Davoodabadi, A. Jazari, Thermal performance of microchannel heat sink integrated with porous medium , slip coefficient and phase change material and machine learning approach, J Energy Storage 74 (2023) 109357. https://doi.org/10.1016/j.est.2023.109357.

[14] Z. Xu, G. Yu, T. Zhang, R. Wang, Cooling performance of battery pack as affected by inlet position and inlet air velocity in electric vehicle, Case Studies in Thermal Engineering 39 (2022) 102382. https://doi.org/10.1016/j.csite.2022.102382.

[15] M. Wang, T.C. Hung, H. Xi, Numerical study on performance enhancement of the air-cooled battery thermal management system by adding parallel plates, Energies (Basel) 14 (2021). https://doi.org/10.3390/en14113096.

[DOI: 10.22068/ase.2024.678]

[16] R.D. Widyantara, M.A. Naufal, P.L. Sambegoro, I.P. Nurprasetio, F. Triawan, D.W. Djamari, A. Bayu, D. Nandiyanto, B.A. Budiman, M. Aziz, Electric Vehicle, (2021).

[17] S. Davoodabadi, A. Davoodabadi, Journal of Magnetism and Magnetic Materials Scrutiny of melting rate of phase change material in a four petals cavity with internal branch fins under magnetic field, 575 (2023) 1–12. https://doi.org/10.1016/j.jmmm.2023.170727.

[18] S. Davoodabadi, A. Davoodabadi, A. Jazari, W. Yan, Evaluation of phase change material melting process in an energy storage chamber with porous metal foam gradient and discrete strip fins, J Energy Storage 56 (2022) 106005. https://doi.org/10.1016/j.est.2022.106005.

[19] H. Wang, T. Tao, J. Xu, X. Mei, X. Liu, P. Gou, Cooling capacity of a novel modular liquid-cooled battery thermal management system for cylindrical lithium ion batteries, Appl Therm Eng 178 (2020) 115591. https://doi.org/10.1016/j.applthermaleng.2020.115591.

[20] P. Li, J. Zhao, S. Zhou, J. Duan, X. Li, H. Zhang, J. Yuan, Design and Optimization of a Liquid Cooling Thermal Management System with Flow Distributors and Spiral Channel Cooling Plates for Lithium-Ion Batteries, Energies (Basel) 16 (2023). https://doi.org/10.3390/en16052196.

[21] M. Magnini, J.R. Thome, A CFD study of the parameters influencing heat transfer in microchannel slug flow boiling, International Journal of Thermal Sciences 110 (2016) 119–136. https://doi.org/10.1016/j.ijthermalsci.2016.06.032.

[22] H. Li, P. Hrnjak, Flow visualization of R1234ze(E) in a 0.643 mm microchannel tube, Int J Heat Mass Transf 136 (2019) 950–961. https://doi.org/10.1016/j.ijheatmasstransfer.2019.03.022.

[23] S.A. Jayarajan, U. Azimov, CFD Modeling and Thermal Analysis of a Cold Plate Design with a Zig-Zag Serpentine Flow Pattern for Li-Ion Batteries by dissipation, (2023).

[24] L. Wei, Y. Zou, F. Cao, Z. Ma, Z. Lu, L. Jin, An Optimization Study on the Operating Parameters of Liquid Cold Plate for Battery Thermal Management of Electric Vehicles, Energies (Basel) 15 (2022). https://doi.org/10.3390/en15239180.

[25] J. Dong, X. Lu, Y. Sun, V. Mitin, H. Xu, W. Kong, Design of Battery Thermal Management System with Considering the Longitudinal and Transverse Temperature Difference, Energies (Basel) 15 (2022). https://doi.org/10.3390/en15197448.

[26] P.S. Lee, S. V. Garimella, Saturated flow boiling heat transfer and pressure drop in silicon microchannel arrays, Int J Heat Mass Transf 51 (2008) 789–

[DOI: 10.22068/ase.2024.678]

806. https://doi.org/10.1016/j.ijheatmasstransfer.2007.04.019.

[27] H. Li, P. Hrnjak, Heat transfer and pressure drop of R32 evaporating in one pass microchannel tube with parallel channels, Int J Heat Mass Transf 127 (2018) 526–540. https://doi.org/10.1016/j.ijheatmasstransfer.2018.08.062.

[28] R. Lin, J. Xie, R. Liang, X. Li, G. Zhang, B. Li, Experiments and Simulation on the Performance of a Liquid-Cooling Thermal Management System including Composite Silica Gel and Mini-Channel Cold Plates for a Battery Module, Energies (Basel) 15 (2022). https://doi.org/10.3390/en15239103.

[29] D. Worwood, J. Marco, Q. Kellner, E. Hosseinzadeh, R. McGlen, D. Mullen, K. Lynn, D. Greenwood, Experimental Analysis of a Novel Cooling Material for Large Format Automotive Lithium-Ion Cells, Energies (Basel) 12 (2019). https://doi.org/10.3390/en12071251.

[30] C. Zhao, B. Zhang, Y. Zheng, S. Huang, T. Yan, Hybrid Battery Thermal Management System in Electrical Vehicles: A Review, (2020).

[31] Y.H. Huang, W.L. Cheng, R. Zhao, Thermal management of Li-ion battery pack with the application of flexible form-stable composite phase change materials, Energy Convers Manag 182 (2019) 9–20. https://doi.org/10.1016/j.enconman.2018.12.064.

[32] V.G. Choudhari, A.S. Dhoble, S. Panchal, M. Fowler, R. Fraser, Numerical investigation on thermal behaviour of 5×5 cell configured battery pack using phase change material and fin structure layout, J Energy Storage 43 (2021) 103234. https://doi.org/10.1016/J.EST.2021.103234.

[33] M. Rabiei, A. Gharehghani, A.M. Andwari, Enhancement of battery thermal management system using a novel structure of hybrid liquid cold plate, Appl Therm Eng 232 (2023) 121051. https://doi.org/10.1016/j.applthermaleng.2023.121051.

[34] S. Ki, J. Lee, S. Kim, J. Seong, J. Shim, S. Oh, S. Cho, S. Bang, D. Seo, J. Kim, Y. Nam, An energy-efficient battery thermal management system incorporating a porous metal-based multiscale flow manifold, Energy Convers Manag 269 (2022) 116147. https://doi.org/10.1016/j.enconman.2022.116147.

[35] J. Weng, Y. He, D. Ouyang, X. Yang, G. Zhang, J. Wang, Thermal performance of PCM and branch-structured fins for cylindrical power battery in a high-temperature environment, Energy Convers Manag 200 (2019) 112106. https://doi.org/10.1016/j.enconman.2019.112106.

[DOI: 10.22068/ase.2024.678]

[36] K. Monika, C. Chakraborty, S. Roy, S. Dinda, S.A. Singh, S.P. Datta, An improved mini-channel based liquid cooling strategy of prismatic LiFePO4 batteries for electric or hybrid vehicles, J Energy Storage 35 (2021) 102301. https://doi.org/10.1016/j.est.2021.102301.

[37] D. Bernardi, E. Pawlikowski, J. Newman, General Energy Balance for Battery Systems., Electrochemical Society Extended Abstracts 84–2 (1984) 164–165. https://doi.org/10.1149/1.2113792.

[38] H. Fathabadi, A novel design including cooling media for Lithium-ion batteries pack used in hybrid and electric vehicles, J Power Sources 245 (2014) 495–500. https://doi.org/10.1016/j.jpowsour.2013.06.160.

[39] W. Li, M. Xiao, X. Peng, A. Garg, L. Gao, A surrogate thermal modeling and parametric optimization of battery pack with air cooling for EVs, Appl Therm Eng 147 (2019) 90–100. https://doi.org/10.1016/j.applthermaleng.2018.10.060.

[40] M.M. Heyhat, M.Q.J. Abbood, J. Ahbabi Saray, A. Mokhtari Ardekani, Comparative assessment of direct absorption solar collector performance in different climates, Sci Rep 13 (2023) 1–17. https://doi.org/10.1038/s41598-023-48780-4.

[41] L. Li, X. Li, Y. Xie, H. Huang, Y. Huang, H. Wang, S. Bei, Q. Xu, X. Wang, K. Zheng, Adaptability enhancement of mini-channel cold plate for cylindrical battery module under various ambient temperatures, Appl Therm Eng 253 (2024) 123682. https://doi.org/10.1016/j.applthermaleng.2024.123682.

[42] C. Lin, K. Chen, F. Sun, P. Tang, H. Zhao, Research on thermo-physical properties identification and thermal analysis of EV Li-ion battery, 5th IEEE Vehicle Power and Propulsion Conference, VPPC '09 (2009) 1643–1648. https://doi.org/10.1109/VPPC.2009.5289653.

[43] L. Fan, J.M. Khodadadi, A.A. Pesaran, A parametric study on thermal management of an air-cooled lithium-ion battery module for plug-in hybrid electric vehicles, J Power Sources 238 (2013) 301–312. https://doi.org/10.1016/j.jpowsour.2013.03.050.

[44] Lin Cheng, Chen Ke, Sun Fengchun, Tang Peng, Zhao Hongwei, Research on thermo-physical properties identification and thermal analysis of EV Li-ion battery, in: 2009 IEEE Vehicle Power and Propulsion Conference, IEEE, 2009: pp. 1643–1648. https://doi.org/10.1109/VPPC.2009.5289653.

[45] E. Hosseinzadeh, R. Genieser, D. Worwood, A. Barai, J. Marco, P.

[DOI: 10.22068/ase.2024.678]

Jennings, A systematic approach for electrochemical-thermal modelling of a large format lithium-ion battery for electric vehicle application, J Power Sources 382 (2018) 77–94. https://doi.org/10.1016/j.jpowsour.2018.02.027.

[DOI: 10.22068/ase.2024.678]